ELSEVIER

Nuclear Instruments and Methods in Physics Research B 179 (2001) 133–144

NIM B
Beam Interactions with Materials & Atoms

www.elsevier.nl/locate/nimb

# Analysis of outputs from a helium-filled proportional counter at liquid helium temperature

Sei Masaoka [a], Rintaro Katano [a], Yasuhito Isozumi [b,*]

[a] *Institute for Chemical Research, Kyoto University, Uji, Kyoto, 611-0011, Japan*
[b] *Radioisotope Research Center, Kyoto University, Kyoto, 606-8501, Japan*

Received 8 September 2000; received in revised form 2 January 2001

**Abstract**

We have formulated output currents from helium-filled proportional counter (HFPC) cooled at low temperatures near 4.2 K, taking account of primary electrons produced by incident radiation and secondary electrons emitted from cathode; according to a simple model for the HFPC operation, the secondary electrons are originated by collision of four active particles with cathode, i.e. low-energy (0–5 eV) photons from excited helium atoms $He^*$, helium ion clusters $He_n^+$, high-energy (10–20 eV) photons from excited helium molecules $He_2^*(A^1\Sigma_u^+)$ and metastable helium molecules $He_2^m(a^3\Sigma_u^+)$. In order to determine secondary electron emission probability for each active particle, output pulses and electric discharges from the HFPC have been analyzed with the theoretical formulation. The present analysis has made clear the roles of low- and high-energy photons and the ion clusters quantitatively. However, the role of triplet metastables, $He_2^m(a^3\Sigma_u^+)$ or $He^m(2^3S)$, is still not clear. The formulation and some results of the analysis are described in detail. A possible application of the HFPC to a new neutron position detector is also proposed. 

*Keywords:* CEMS; Proportional counter; Low temperature; Liquid helium

## 1. Introduction

Resonance-electron Mössbauer spectroscopy (REMS) or conversion-electron Mössbauer spectroscopy (CEMS) is intensively applied to investigations of surface layer of metals, alloys and chemical compounds including iron, tin and europium [1–4]. The helium-filled proportional counter (HFPC) makes possible to perform cryogenic REMS measurements; HFPC can be employed to detect electrons resonantly scattered from samples cooled at low temperatures near 4.2 K [3–7].

The HFPC operates in the proportional region at the low temperatures in spite of containing no quenching admixture such as organic gases. However, the self-sustained electric discharge is induced at rather low gas gains of 200 at most [8].

* Corresponding author. Tel. +81-75-753-7512; fax: +81-75-753-7504.
*E-mail address:* yasuhito@barium.rirc.kyoto-u.ac.jp (Y. Isozumi).

0168-583X/01/$ - see front matter 
PII: S0168-583X(01)00328-7

The operation is practically limited by the discharge. In our previous work [9], a model for the operation of HFPC at the low temperatures was constructed by comparing experimental observations of after-pulses and electric discharge with fundamental collision processes in helium gas.

There are two main conclusions deduced from the model:

1. Atom–atom and atom–molecule collisions in helium gas are remarkably suppressed at low temperatures near 4.2 K. A dominant process in electron avalanches is the ionization by electron impact and the contribution of the collisional ionization of highly excited helium $He^*(n \geqslant 3)$, i.e., the so-called Hornbeck–Molnar process [10] becomes negligibly small at the low temperatures.
2. Four active particles are generated in the operation of HFPC which emit secondary electrons through the collision with cathode material, i.e. low-energy (0–5 eV) photons from excited helium atoms $He^*$, helium ion clusters $He_n^+$, high-energy (10–20 eV) photons from excited helium molecules $He_2^*(A^1\Sigma_u^+)$ and metastable helium molecules $He_2^m(a^3\Sigma_u^+)$. The secondary electrons from cathode cause the after-pulse [11] and the electric discharge [12].

Using the theoretical treatment for the proportional counter operation [13] and the electric discharge in gas [14], output signals from HFPC (including electric discharge) can be deduced from the model explained above. We have first derived the theoretical expression for the output signals in the present work. Second, we have experimentally observed output signals for various values of anode voltage and helium gas density at 4.2 K. Finally, the probability of the secondary electron emission caused by each active particle has been determined from the careful simulation of the experimental data with the theoretical expression. As a result of the present analysis, it is proved that $He_2^*(A^1\Sigma_u^+)$ and $He_2^m(a^3\Sigma_u^+)$ give much larger influence on the unfavorable operation of HFPC than the other two active particles. The helium gas density of HFPC examined by the present work is rather low, i.e. up to 32 Torr at 4.2 K. The analysis indicates that the HFPC may operate in the region of higher gas densities. In this paper a possibility of high-resolution neutron position detector as an application of the HFPC is also discussed.

In Section 2 the theoretical formulation for output signals from HFPC, which is inevitable in the present analysis, is explained in detail. The experimental procedure and the output signals observed are given in Section 3. Details of the data analysis are given in Section 4. Some new aspects on atomic and molecular processes in the HFPC operation are discussed in Section 5. A future work on the neutron position detector and concluding remarks are given in Section 6.

## 2. Theoretical formulation of electric current from HFPC

### 2.1. Current caused by incident radiation

In proportional counters, incident radiation ionizes filling gas to produce pairs of electrons and positive ions. The number of pairs are proportional to the radiation energy deposited in the gas. Primary electrons produced in the ionization successively ionize gas atoms or molecules after they are attracted to the anode and accelerated by the steep electric field near the anode. Each electron finally grows up to an avalanche whose average electron number is defined as gas gain $G$. Thus, the number of primary electrons is multiplied by a factor $G$ in the electron avalanche.

The electric charge from the proportional counter is mainly induced by the positive ions; they are created at the position with the strongest electric field, i.e. near anode wire, and immediately move from there to cathode. The output current for cylindrical counters [15] is given by

$$I_0(t) = \frac{Q_0}{t + T_0} \quad \text{for } t < T_i, \tag{1a}$$

$$= 0 \quad \text{for } T_i < t, \tag{1b}$$

where $T_0$ is a parameter related to the velocity of positive ions and $T_i$ is their drift time from anode to cathode. The parameter $T_0$ is the order of 0.5 ns and $T_i$ is 200–600 μs, depending on counter geometry, filling gas and anode voltage. The charge $Q_0$ is defined by $GN_0e$, where $N_0$ is the number of

electrons produced by the primary ionization and $e$ is the charge of an electron.

### 2.2. Current caused by active particles

There are three kinds of active particles created in electron avalanches, which can arrive at the cathode and emit secondary electrons through the collision with cathode material, i.e. ultraviolet photons, positive ions and metastables. According to our previous work [9], active particles appearing in the operation of HFPC are photons from excited helium atoms $He^*$, helium ion clusters $He_n^+$, photons from excited helium molecule $He_2^*(A^1\Sigma_u^+)$ and metastable helium molecule $He_2^m(a^3\Sigma_u^+)$. The secondary electrons emitted by those active particles travel to the anode and generate new avalanches there.

There is a distinct delay in time between avalanches by primary electrons and those by secondary electrons. The delay of charged particles, i.e. electrons and positive ions, results from their drift between the anode and cathode while that of neutral particles, i.e. metastables, results from their diffusion. The time delay is given by a sum of $T_\gamma + T_e(=\sim T_e)$ for photons, $T_i + T_e(=\sim T_i)$ for positive ions and $T_M + T_e(=\sim T_M)$ for metastables, where $T_\gamma$ is the time interval for the photons to travel from the anode to the cathode, $T_e$ and $T_i$ are the drift time for electrons and positive ions, respectively, and $T_M$ is the diffusion time for metastables. A typical value for each time interval is $T_\gamma = 0.5$ ns, $T_e = 2$–$3$ μs, $T_i = 200$–$600$ μs and $T_M = 1$–$10$ ms. Therefore, the output current induced by primary electrons is successively superimposed by additional currents, which are induced by secondary electrons from cathode. These additional currents are usually suppressed by adding some quencher, e.g. organic gas such as $CH_4$ and $C_4H_{10}$, in helium. All quenchers are frozen at low temperatures near 4.2 K. Because of the complete lack of quenchers in HFPC at the low temperatures, its proportional-counter operation is harmed by the additional currents, as seen below.

#### 2.2.1. Helium ion clusters

Positive helium ions $He^+$ produced in avalanches are immediately turned into molecular helium ions $He_2^+$ through the three-body collision with helium atoms He. Especially at the low temperatures they are changed into helium ion clusters $He_n^+$ by repetition of the three-body collisions in their drift to cathode [16]. The ion clusters emit secondary electrons by colliding with the cathode, which cause new electron avalanches with a time delay of $T_i$.

#### 2.2.2. Photons from excited helium atom

Excited helium atoms, $He^*$, produced in electron avalanches decay to lower states both through radiative transitions and collisions with helium gas atoms, He. As shown in the previous work [9], the rate of the collisional de-excitation is decreased at low temperatures near 4.2 K. Therefore, the rate of the radiative transition is comparatively enhanced at the temperatures. Photons emitted by the transition to the ground are resonantly re-absorbed by He [17]. A part of $He^*$ produced by the resonance absorption again decays to the ground emitting the resonance photons (∼20 eV), while the other part decays to lower states emitting low-energy photons (∼5 eV). The resonance photons disappear through repetition of the absorption by He before reaching the cathode. The low-energy photons, called non-resonance photons, arrive at the cathode without being absorbed by He. Thus, the non-resonance photons give rise to photo-ionizations at the cathode. Secondary electrons produced by the photo-ionizations induce new electron avalanches at the anode with a time delay of $T_e$.

#### 2.2.3. Photons from excited molecule $He_2^*(A^1\Sigma_u^+)$

Singlet metastable helium atoms $He^m(2^1S)$ are changed to excited helium molecules $He_2^*(A^1\Sigma_u^+)$ through two-body or three-body collisions with helium gas atoms He [18]. The $He_2^*(A^1\Sigma_u^+)$ molecules emit non-resonance photons through radiative decays, with energies higher than those from excited helium atoms $He^*$,

$$He^m(2^1S) + He \rightarrow He_2^*(A^1\Sigma_u^+), \quad (2a)$$

$$He_2^*(A^1\Sigma_u^+) \rightarrow 2He + h\nu \ (20.5\text{–}20.6 \text{ eV}). \quad (2b)$$

$$He^m(2^1S) + 2He \rightarrow He_2^*(A^1\Sigma_u^+) + He, \quad (3a)$$

$$He_2^*(A^1\Sigma_u^+) \rightarrow He_2^*(X^1\Sigma_g^+) + h\nu \ (11.2\text{–}20.6 \text{ eV}). \quad (3b)$$

The reaction rates of the collisions (2a) and (3a) are $1.7 \times 10^5$ and $8.1 \times 10^5$ $s^{-1}$, respectively, at normal condition (760 Torr at room temperature) [19]. Accordingly, the lifetime of $He^m(2^1S)$ becomes the order of μs at the normal condition, while its intrinsic lifetime is 20 ms [20]. This suggests that a large part of $He^m(2^1S)$ produced in electron avalanches is changed to $He_2^*(A^1\Sigma_u^+)$.

*2.2.4. Metastable molecules* $He_2^m(a^3\Sigma_u^+)$

Triplet metastable helium atoms $He^m(2^3S)$ are changed to metastable molecules $He_2^m(a^3\Sigma_u^+)$ through three-body collisions with helium gas atoms He [21],

$$He^m(2^3S) + 2He \rightarrow He_2^m(a^3\Sigma_u^+) + He. \quad (4)$$

The reaction rate is $1.5 \times 10^5$ $s^{-1}$ at normal condition while the intrinsic lifetime of $He^m(2^3S)$ is very long, i.e. $6 \times 10^5$ s [20]. Therefore, a large part of $He^m(2^3S)$ produced in electron avalanches is changed to $He_2^m(a^3\Sigma_u^+)$. The metastables $He_2^m(a^3\Sigma_u^+)$ diffuse from anode to cathode with a diffusion time, $T_M$, which is the order of 1–10 ms. They are decomposed into pairs of two He by emitting secondary electrons from the cathode, which cause new electron avalanches with a time delay of $T_M$.

*2.2.5. Theoretical expression for the current by active particles*

The electric current from the new avalanches, caused by one of the active particles, is given by

$$i_a(T,t) = \frac{Q_a(T)}{t - T + T_0} \quad \text{for } T < t < T + T_i, \quad (5a)$$

$$= 0 \quad \text{for } t < T, T + T_i < t. \quad (5b)$$

In the above expression, the subscript $a$ is i, p1, p2 or m indicating the active particle $He_n^+$, photons from $He^*$, photons from $He_2^*(A^1\Sigma_u^+)$ or $He_2^m(a^3\Sigma_u^+)$, respectively. The notation $T$ ($> T_i$, $T_{p1}$, $T_{p2}$ or $T_m$) is a time when the secondary electrons, emitted by the collision of active particles with cathode, induce new avalanches and $Q_a(T)$ is the total charge induced in the avalanches at the time $T$.

*2.3. Electric charges induced in electron avalanches*

The total electric charges induced on the anode is a sum of charges in electron avalanches caused by primary electrons, which are created by an incident radiation, and those by secondary electrons, which are emitted by collisions of the active particles with the cathode,

$$Q(T) = Q_0\delta(T) + Q_i(T) + Q_{p1}(T) + Q_{p2}(T) + Q_m(T), \quad (6)$$

where $Q_0$ is defined in Eq. (1) and $Q_i(T)$, $Q_{p1}(T)$, $Q_{p2}(T)$ and $Q_m(T)$ are defined in Eq. (5). Using the step function $\theta(t)$, the charges $Q_i(T)$ and $Q_{p1}(T)$ are, respectively, expressed by

$$Q_i(T) = R_i Q(T - T_i)\theta(T - T_i), \quad (7)$$

$$Q_{p1}(T) = R_{p1} Q(T - T_e)\theta(T - T_e), \quad (8)$$

where $R_i$ is defined as the probability of the secondary electron emission caused by helium ion cluster $He_n^+$ and $R_{p1}$ is defined as that caused by photons from excited helium $He^*$ [14]. The probabilities $R_i$ and $R_{p1}$ are, respectively, given by

$$R_i = G\Gamma_i, \quad (9)$$

$$R_{p1} = GP_{p1}\varepsilon_{p1}\Gamma_{p1}. \quad (10)$$

In the above expressions, $G$ is the gas gain and $\Gamma_i$ is the second Townsend ionization coefficient of the positive ion. The parameter $P_{p1}$ is the relative population of $He^*$ per ionization event in an avalanche, $\varepsilon_{p1}$ is a ratio of the reaction rate of the photon production to that of all decaying processes for $He^*$ and $\Gamma_{p1}$ is the second Townsend ionization coefficient for the photons [9].

As discussed before, the lifetime of $He^m(2^1S)$ is of the order of μs in helium gas at the normal condition. However, the frequency of the collision processes (2a) and (3a) becomes smaller at 4.2 K and the lifetime becomes much longer than that at room temperature. As a consequence, $He_2^*(A^1\Sigma_u^+)$ produced from $He^m(2^1S)$ has a time spread of the order of 100 μs and new electron avalanches induced also have a spread of the same order. The rate of $He_2^*(A^1\Sigma_u^+)$ produced at a time $t_p$ later after the production of $He^m(2^1S)$ is expressed by $(1/T_P)\exp(-t_p/T_P)$, where $T_P$ is an average of the

time spread. Since the photons from $He_2^*(A^1\Sigma_u^+)$ induce electron avalanches at a time $T_e$ later, the total time delay is the sum of $T_e$ and $t_p$. The electric charge induced in avalanches at a time $T + T_e + t_p$ is approximately given by

$$q_{p2}(T + T_e + t_p) = R_{p2}Q(T)p_p(t_p), \tag{11}$$

where

$$p_p(t) = \frac{1}{T_p}\exp\left(-\frac{t}{T_P}\right). \tag{12}$$

Eq. (11) is transformed as

$$q_{p2}(T, t_p) = R_{p2}Q(T - T_e - t_p)p_p(t_p), \tag{13}$$

where $R_{p2}$ is defined as the average number of electron avalanches caused by $He_2^*(A^1\Sigma_u^+)$,

$$R_{p2} = GP_{p2}\varepsilon_{p2}\Gamma_{p2}, \tag{14}$$

where $P_{p2}$, $\varepsilon_{p2}$ and $\Gamma_{p2}$ are similarly defined as those in Eq. (9). The total charge $Q_{p2}(T)$ at a time $T$ is given by an integral of Eq. (11) with regard to $t_p$,

$$Q_{p2}(T) = R_{p2}\int_0^{T-T_e} Q(T - T_e - t_p)p_p(t_p)\theta(T - T_e - t_p)\,dt_p. \tag{15}$$

For simplicity in calculation, this integral is transformed into a summation as

$$Q_{p2}(T) = R_{p2}\sum_{k=0}^{\lfloor (T-T_e)/\Delta t\rfloor} Q(T - T_e - k\Delta t)f_p(k) \times \theta(T - T_e - k\Delta t), \tag{16}$$

$$f_p(k) = \frac{1}{T_P}\int_{k\Delta t}^{(k+1)\Delta t}\exp\left(-\frac{x}{T_P}\right)dx. \tag{17}$$

Similar to $He_2^*(A^1\Sigma_u^+)$, $He_2^m(a^3\Sigma_u^+)$ is also produced through the collisional reaction (4) with a time spread of the order of 100 μs. As discussed in Section 2.2.4, $He_2^m(a^3\Sigma_u^+)$ travels to the cathode by diffusion. Since the diffusion time is the order of 1–10 ms, which is much larger than the time spread, a time delay of the after-pulse is approximately given by the diffusion time $T_M$. The total charge caused by $He_2^m(a^3\Sigma_u^+)$ is expressed as

$$Q_m(T) = R_m\int_0^T Q(T - T_M)p_m(T_M)\theta(T - T_M)\,dT_M, \tag{18}$$

$$p_m(t) = \frac{b}{\sqrt{8D}}\frac{1}{t^{3/2}}\exp\left(-\frac{\pi b^2}{8Dt}\right). \tag{19}$$

The function $p_m(t)$ is the probability density of the diffusion current of $He_2^m(a^3\Sigma_u^+)$ near cathode at a time $t$. The parameter $b$ is the radius of the cathode and $D$ is the diffusion coefficient of $He_2^m(a^3\Sigma_u^+)$ in helium gas. By transforming the integral in Eq. (18) into summation, we obtain

$$Q_m(T) = R_m\sum_{k=0}^{\lfloor (T-T_m)/\Delta t\rfloor} Q(T - T_m - k\Delta t)f_m(k) \times \theta(T - T_m - k\Delta t), \tag{20}$$

$$f_m(k) = \frac{b}{\sqrt{8D}}\int_{T_m+k\Delta t}^{T_m+(k+1)\Delta t}\frac{1}{t^{3/2}}\exp\left(-\frac{\pi b^2}{8Dt}\right)dt, \tag{21}$$

$$R_m = GP_m\varepsilon_m\Gamma_m, \tag{22}$$

where $T_M$ is replaced by $T_m + k\Delta t$. The parameter $T_m$ is defined as the shortest time in which $He_2^m(a^3\Sigma_u^+)$ created near the anode arrive at the cathode. Parameters in Eq. (22) are similarly defined as those in Eq. (10).

### 2.4. Total current from HFPC

Corresponding to the total electric charges given by Eq. (6), the electric current from HFPC is expressed as

$$I(t) = I_0(t) + \sum_{k=0}^{\lfloor t/\Delta t\rfloor}\left\{i_i(k\Delta t, t) + i_{p1}(k\Delta t, t) + i_{p2}(k\Delta t, t) + i_m(k\Delta t, t)\right\}, \tag{23a}$$

$$= I_0(t) + \sum_{k=0}^{\lfloor t/\Delta t\rfloor}\left\{i_i(k\Delta t, t) + i_{p1}(k\Delta t, t)\right\} + \sum_{k=0}^{\lfloor (t-T_e)/\Delta t\rfloor} j_{p2}(k, t) + \sum_{k=0}^{\lfloor (t-T_m)/\Delta t\rfloor} j_m(k, t), \tag{23b}$$

where $I_0(t)$ is given by Eq. (1) and $i_i(T,t)$, $i_{p1}(T,t)$, $i_{p2}(T,t)$ and $i_m(T,t)$ are given by Eq. (5). The currents $i_{p2}(k,t)$ and $i_m(k,t)$ in Eq. (23a) are reformed to $j_{p2}(k,t)$ and $j_m(k,t)$ in Eq. (23b) according to Eqs. (16) and (20), respectively. An explicit expression of $j_{p2}(k,t)$ is given by

$$j_{p2}(k,t) = 0 \quad \text{for } t < k\Delta t, \tag{24a}$$

$$= \sum_{s=0}^{\lfloor (t-T_e)/\Delta t\rfloor - k} \frac{R_{p2}Q(k\Delta t)f_p(s)}{t - T_e - (k+s)\Delta t + T_0} \tag{24b}$$

$$\text{for } T_e + k\Delta t < t < T_e + k\Delta t + T_i,$$

$$= \sum_{s=\lfloor (t-T_e-T_i)/\Delta t\rfloor - k + 1}^{\lfloor (t-T_e)/\Delta t\rfloor - k} \frac{R_{p2}Q(k\Delta t)f_p(s)}{t - T_e - (k+s)\Delta t + T_0}$$

$$\text{for } T_e + k\Delta t + T_i < t. \tag{24c}$$

The current $j_m(k,t)$ is obtained by replacing $T_e$, $R_{p2}$ and $f_p(s)$ in Eq. (24) with $T_m$, $R_m$ and $f_m(s)$, respectively.

### 2.5. Output voltage from a charge-sensitive preamplifier

When the delta function is fed to a charge-sensitive preamplifier, its transfer function is given by

$$W(p;\ \text{impulsive}) = \frac{1}{C_f}\frac{1}{p + 1/T_f}, \tag{25}$$

where $T_f$ is the time constant of the preamplifier and $C_f$ is the capacitance of feed-back loop [12]. Then, the impulsive response of the preamplifier is expressed by

$$W(t) = -\frac{1}{C_f}\exp\left(-\frac{t}{T_f}\right). \tag{26}$$

For the total current from HFPC, i.e. $I(t)$ given by Eq. (23), the output voltage of the preamplifier, $V(t)$, is expressed by

$$V(t) = [W(t)] \otimes [I(t)]$$

$$= \frac{1}{C_f}\exp\left(-\frac{t}{T_f}\right)\int_0^t \exp\left(\frac{x}{T_f}\right) I(x)\,dx, \tag{27}$$

where the symbol $\otimes$ indicates the convolution between $W(t)$ and $I(t)$. The explicit expression of $V(t)$ is

$$V(t) = V_0(t) + \sum_{k=0}^{\lfloor (t-T_i)/\Delta t\rfloor} R_i Q(k\Delta t) v_r(k\Delta t, t)$$

$$+ \sum_{k=0}^{\lfloor (t-T_e)/\Delta t\rfloor} Q(k\Delta t)\left\{R_{p1}v_r(k\Delta t,t) + R_{p2}v_p(k\Delta t,t)\right\}$$

$$+ \sum_{k=0}^{\lfloor (t-T_m)/\Delta t\rfloor} R_m Q(k\Delta t) v_m(k\Delta t, t), \tag{28}$$

where $V_0(t)$ is given by

$$V_0(t) = \frac{Q_0}{C_f}\exp\left(-\frac{t+T_0}{T_f}\right) \times \int_{T_0}^{t+T_0} \frac{\exp(s/T_f)}{s}\,ds \quad 0 \leqslant t < T_i, \tag{29a}$$

$$= \frac{Q_0}{C_f}\exp\left(-\frac{t+T_0}{T_f}\right) \times \int_{T_0}^{T_i+T_0} \frac{\exp(s/T_f)}{s}\,ds \quad T_i \leqslant t. \tag{29b}$$

The functions $v_r(T,t)$, $v_p(T,t)$ and $v_m(T,t)$ in Eq. (27) are

$$v_r(T,t) = 0 \quad 0 \leqslant t \leqslant T, \tag{30a}$$

$$= \frac{1}{C_f}\exp\left(-\frac{t-T+T_0}{T_f}\right) \times \int_{T_0}^{t-T+T_0} \frac{\exp(s/T_f)}{s}\,ds \tag{30b}$$

$$T < t \leqslant T + T_i,$$

$$= \frac{1}{C_f}\exp\left(-\frac{t-T+T_0}{T_f}\right) \times \int_{T_0}^{T_i+T_0} \frac{\exp(s/T_f)}{s}\,ds \tag{30c}$$

$$T + T_i < t,$$

$$v_p(T,t) = 0 \quad 0 \leqslant t \leqslant T, \tag{31a}$$

$$= \frac{1}{C_f}\exp\left(-\frac{t-T+T_0}{T_f}\right) \times \sum_{k=0}^{\lfloor (t-T_e-T)/\Delta t\rfloor - 1} f_p(k)\exp\left(\frac{k\Delta t}{T_f}\right) \times \int_{T_0}^{t-T_e-T-k\Delta t+T_0} \frac{\exp(s/T_f)}{s}\,ds$$

$$T < t \leqslant T + T_{\mathrm{i}}, \tag{31b}$$

$$= \frac{1}{C_{\mathrm{f}}} \exp\left(-\frac{t - T + T_0}{T_{\mathrm{f}}}\right) \times \left\{ \sum_{k=0}^{\lfloor (t-T_{\mathrm{e}}-T-T_{\mathrm{i}})/\Delta t \rfloor - 1} f_{\mathrm{p}}(k) \exp\left(\frac{k\Delta t}{T_{\mathrm{f}}}\right) \times \int_{T_0}^{T_{\mathrm{i}}+T_0} \frac{\exp(s/T_{\mathrm{f}})}{s}\, \mathrm{d}s + \sum_{k=\lfloor (t-T_{\mathrm{e}}-T-T_{\mathrm{i}})/\Delta t \rfloor}^{\lfloor (t-T_{\mathrm{e}}-T)/\Delta t \rfloor - 1} f_{\mathrm{p}}(k) \exp\left(\frac{k\Delta t}{T_{\mathrm{f}}}\right) \times \int_{T_0}^{t-T_{\mathrm{e}}-T-k\Delta t+T_0} \frac{\exp(s/T_{\mathrm{f}})}{s}\, \mathrm{d}s \right\}$$

$$T + T_{\mathrm{i}} < t. \tag{31c}$$

The expression of $v_{\mathrm{m}}(T,t)$ is similar to that of $v_{\mathrm{p}}(T,t)$, which is obtained by replacing $f_{\mathrm{p}}(k)$ and $T_{\mathrm{e}}$ in Eq. (31) with $f_{\mathrm{m}}(k)$ and $T_{\mathrm{m}}$, respectively.

## 3. Apparatus and experiment

The counter assembly employed in this work is the same as that in the previous work [9] except that nickel is used as a cathode material instead of stainless steel. The preamplifier is commercially available, i.e. CANBERRA 2003T; its decay time constant is 290 μs. We have observed voltage signals from the preamplifier as a function of the helium gas density, $d_{\mathrm{He}}$, and the anode voltage, $V_{\mathrm{a}}$. These outputs have been registered in the digital oscilloscope (Tektronix TDS-220). Incident radiation is 5.3-MeV α-rays from a $^{210}$Po source mounted inside a small collimator, as seen in Fig. 1 of [9]; the direction of α-ray beam is parallel to anode wire. The pulse rate of α-rays is about 1 $\mathrm{s}^{-1}$.

The signals observed are given in Figs. 1 and 2: $d_{\mathrm{He}}$, 10.6 Torr at 4.2 K; $V_{\mathrm{a}}$, 1100, 1200, 1250 and 1300 V. Fig. 1 shows the whole pulse shapes of the signals while Fig. 2 shows their rise parts. It is seen in both figures that there appear after-pulses as bumps, of which the time delay is about 200–250 μs in Fig. 1 and about 2 μs in Fig. 2.

The electric discharges observed as a function of gas density are given in Fig. 3: $d_{\mathrm{He}}$, 10.6, 21 and 32 Torr at 4.2 K. The discharge curve cannot be expressed as a single exponential; the curve is deconvoluted by some exponentials, as described in the previous work [12]. Note that the increasing rate of the curve becomes larger when $d_{\mathrm{He}}$ is increased.

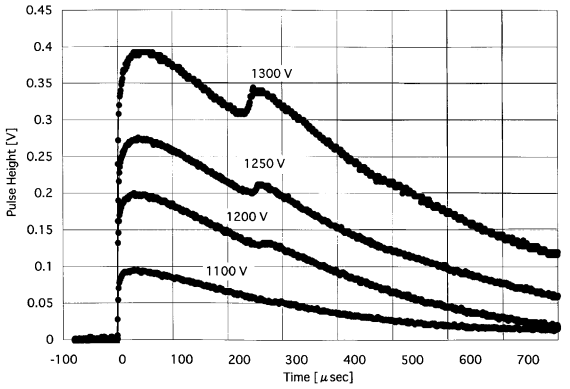


Fig. 1. Output signals observed with $d_{\mathrm{He}} = 10.6$ Torr at 4.2 K; after-pulses appearing at about 200–250 μs later are caused by the collision of positive helium ion clusters $\mathrm{He}_n^+$ with cathode materials.

## 4. Data analysis

### 4.1. Output pulse

According to Section 2.2.4, the new electron avalanches by $\mathrm{He}_2^{\mathrm{m}}(\mathrm{a}^3\Sigma_{\mathrm{u}}^+)$ are induced several ms

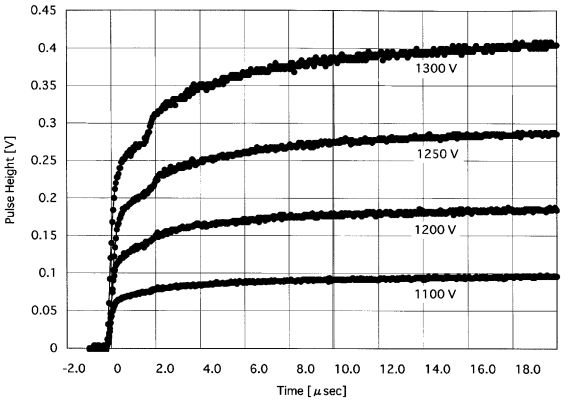


Fig. 2. Rising edges of output signals observed with $d_{\mathrm{He}} = 10.6$ Torr at 4.2 K; after-pulses appearing at about 2 μs are caused by non-resonance photons from the radiative transitions of highly excited helium atoms $\mathrm{He}^*$.

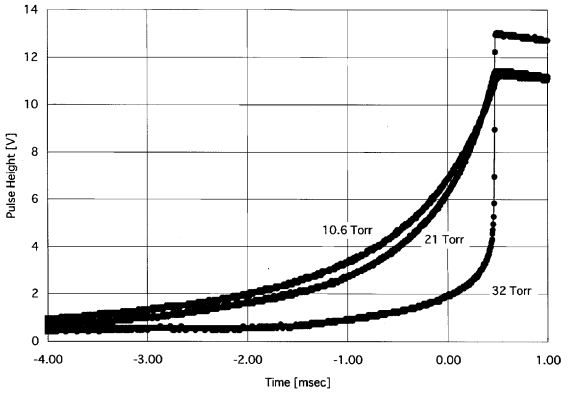


Fig. 3. Self-sustained electric discharge observed with $d_{He} = 10.6$, 21 and 32 Torr at 4.2 K.

later after the start time of radiation signals. Therefore, the last term in Eq. (27), which corresponds to the output voltage caused by $He_2^m(a^3\Sigma_u^+)$, can be neglected in the theoretical simulation for a pulse of radiation signal. The values of $R_{p1}$, $R_{p2}$ and $R_i$ have been determined by reproducing experimental pulses with Eq. (27). In Figs. 4 and 5 typical results of the present simulation are shown. The experimental data are given by closed circles while the simulation result is shown by solid curves: the anode voltage $V_a$, 1300 V; the helium gas density $d_{He}$, 10.6 Torr at 4.2 K. A whole pulse is given in Fig. 4 while a rising edge is given in Fig. 5. It is seen that the output pulses observed agree well with the simulation result. Small differences appearing at the bumps in Fig. 4 and also at the rising edge (0–1 μs) in Fig. 5 are caused by the time fluctuation in the drift of cluster ions and electrons, respectively.

The output pulses can be divided into main pulse and after-pulses. Curve (a) in Figs. 4 and 5 is the main pulse by primary electrons, curve (b) is the after-pulse by helium ion clusters $He_n^+$, curve (c) is that by photons from excited helium $He^*$ and curve (d) is that by photons from excited helium $He_2^*(A^1\Sigma_u^+)$. The values of $R_{p1}$, $R_{p2}$ and $R_i$, determined by the simulation, are given by Table 1. These values increase with increasing anode voltage, as expected. The value of $R_{p2}$ is larger than those of $R_{p1}$ and $R_i$, indicating that the photons from $He_2^*(A^1\Sigma_u^+)$ give a larger influence to the creation of secondary electrons than other active particles, i.e. the photons from $He^*(n \geqslant 3)$ and the cluster ions $He_n^+$.

The time spread for the creation of $He_2^*(A^1\Sigma_u^+)$, $T_P$, discussed in Section 2.3, has been estimated to be 180 μs from the present simulation. The relative error of $T_P$ is 20–30%, which corresponds to the uncertainty of ±0.01 for $R_{p1}$, $R_{p2}$

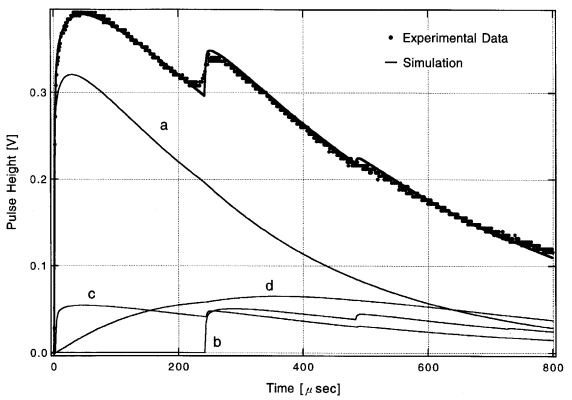


Fig. 4. Simulation for the signal pulse observed with $V_a = 1300$ V and $d_{He} = 10.6$ Torr at 4.2 K. The simulation curve is divided into main pulse and after-pulses: (a) main pulse; (b) after-pulse by helium ion clusters $He_n^+$; (c) after-pulse by photons from excited helium atom $He^*$; (d) after-pulse by photons from $He_2^*(A^1\Sigma_u^+)$.

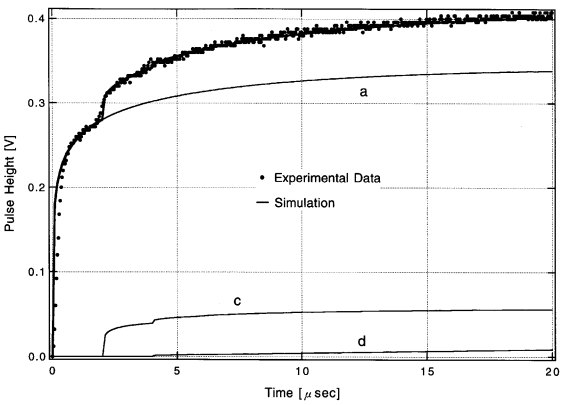


Fig. 5. Simulation for the rising edge of the signal pulse observed with $V_a = 1300$ V and $d_{He} = 10.6$ Torr at 4.2 K. The simulation curve is divided into main pulse and after-pulses: (a) main pulse; (c) after-pulse by photons from excited helium atom $He^*$; (d) after-pulse by photons from $He_2^*(A^1\Sigma_u^+)$.

Table 1
Results of the present simulation (gas temperature: 4.2 K)

| Pressure (Torr) | Anode voltage (V) | $T_e$ (μs) | $T_i$ (μs) | $R_{p1}$ | $R_{p2}$ | $R_i$ | $R_m$ [a] | $R$ [b] |
|---|---|---|---|---|---|---|---|---|
| 10.6 | 1200 | 2.0 | 260 | 0.07 | 0.11 | 0.05 | – | – |
| | 1250 | 2.0 | 250 | 0.09 | 0.20 | 0.08 | – | – |
| | 1300[c] | 2.0 | 240 | 0.14 | 0.23 | 0.13 | ~0.50 | ~1.0 |
| 21 | 1300 | 2.4 | 470 | 0.06 | 0.18 | 0.07 | – | – |
| | 1400 | 2.4 | 440 | 0.11 | 0.20 | 0.17 | – | – |
| | 1430[c] | 2.4 | 425 | 0.12 | 0.21 | 0.20 | ~0.47 | ~1.0 |
| 32 | 1400 | 3.0 | 645 | 0.05 | 0.14 | 0.06 | – | – |
| | 1500 | 3.0 | 600 | 0.08 | 0.19 | 0.10 | – | – |
| | 1550[c] | 3.0 | 590 | 0.12 | 0.30 | 0.25 | ~0.33 | ~1.0 |

[a] Estimated from $(1 - R_{p1} - R_{p2} - R_i)$.
[b] $R \equiv R_{p1} + R_{p2} + R_i + R_m$.
[c] Maximum available anode voltage, $V_{max}$.

and $R_i$. As shown by curve (d) in Fig. 4, the rising edge of the after-pulse by $He_2^*(A^1\Sigma_u^+)$ is very slow because of the large time spread, $T_p$.

When the sum of the electron emission probabilities, i.e. $R$ $(\equiv R_i + R_{p1} + R_{p2} + R_m)$, becomes larger than unity, the electric discharge takes place. In the present work, the signal pulses have been observed by applying the maximum available anode voltage, $V_{max}$, which does not induce the electric discharge but certainly induces the discharge by being made higher by about 10 V. Therefore, $R$ is nearly unity for the signal pulses observed at $V_a = V_{max}$. Thus, the $R_m$ values at $V_a = V_{max}$ can be deduced as

$$R_m \sim 1 - (R_{p1} + R_{p2} + R_i). \quad (32)$$

The values of $R_m$ are also listed in Table 1.

### 4.2. Electric discharge

The last term in Eq. (27) should be taken into account in order to calculate a theoretical shape of an electric discharge. The experimentally observed discharge shape (closed circle) and the simulation results (solid curves) for $V_a = 1300$ V and $d_{He} = 10.6$ Torr at 4.2 K are shown in Fig. 6. Since the diffusion coefficient $D$ for $He_2^m(a^3\Sigma_u^+)$, which is necessary to estimate the last term, has not been reported, the value is assumed to be a reasonable value, i.e. $6 \times 10^{-2}$ m$^2$/s, in the present work. The values of $R_{p1}$, $R_{p2}$ and $R_i$ used in the simulation are 0.14, 0.23 and 0.13, respectively, as seen in Table 1. The four curves in Fig. 6 are the simulation results obtained with $R_m = 0.55$, 0.60, 0.65 and 0.70, respectively. All curves are approximately expressed as an exponential function when the time is sufficiently large. The difference between the experimental data and the simulation is apparently large;

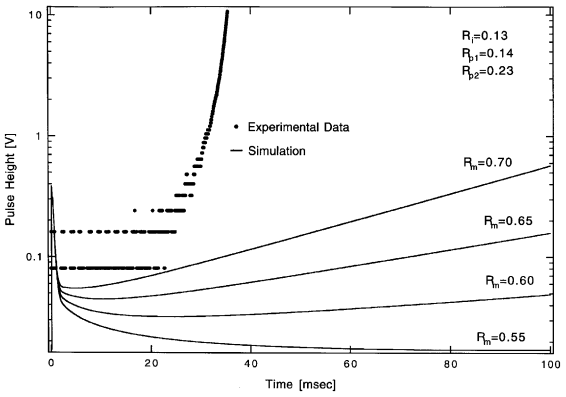


Fig. 6. Simulations for the electric discharge observed with $V_a = 1300$ V and $d_{He} = 10.6$ Torr at 4.2 K. All simulation curves, which have been calculated with $R_m = 0.55$, 0.60, 0.65 and 0.70, do not agree with the experimental data.

the experimental curve increases much more rapidly than all the curves. This indicates that the present model for the electric discharge is not sufficient and there may exist another mechanism to induce the discharge. A possible mechanism is discussed later.

## 5. Discussion

We have tried to estimate the parameters $P$, $\varepsilon$ and $\Gamma$ in the expressions of $R_i$, $R_{p1}$, $R_{p2}$ and $R_m$, i.e. Eqs. (9), (10), (14) and (22), respectively. It is possible to perform such an estimation for the $R$ values obtained at $V_a = V_{max}$. Typical results for $d_{He} = 10.6$ Torr at 4.2 K are listed in Table 2. Results for other densities, i.e. $d_{He} = 21$ and 32 Torr at 4.2 K, are almost the same as that for $d_{He} = 10.6$ Torr.

Table 2
Estimation for parameters in $R_i$, $R_{p1}$, $R_{p2}$, and $R_m$

| Parameters | Probable values | |
|---|---|---|
| | 4.2 K (10.6 Torr) | Room temp. (760 Torr) |
| $G$ | 200[a] | 5.6 |
| $R_i[\equiv G\Gamma_i]$ | 0.13[b] | 0.72[c] |
| $\Gamma_i$ | $2.5 \times 10^{-3}$[d] | 0.13[e] |
| $R_{p2}[\equiv GP_{p1}\varepsilon_{p1}\Gamma_{p1}]$ | 0.14[b] | $1 \times 10^{-5}$ |
| $P_{p1}$ | 0.2–0.4[f] | 0.2–0.4[f] |
| $\varepsilon_{p1}$ | 0.1[d] | $1 \times 10^{-3}$[d] |
| $\Gamma_{p1}$ | 0.01[g] | 0.01[g] |
| $R_{p2}[\equiv GP_{p2}\varepsilon_{p2}\Gamma_{p2}]$ | 0.23[b] | 0.06 |
| $P_{p2}$ | 0.1[f] | 0.1[f] |
| $\varepsilon_{p2}$ | 0.1[c] | 0.1[c] |
| $\Gamma_{p2}$ | 0.1[d] | 0.1[d] |
| $R_m[\equiv GP_{pm}\varepsilon_{pm}\Gamma_{pm}]$ | 0.5[b] | 0.22 |
| $P_m$ | 0.2[f] | 0.2[f] |
| $\varepsilon_m$ | 1[c] | 1[c] |
| $\Gamma_m$ | 0.01[d] | 0.2[h] |

[a] Ref. [8].
[b] The present simulation.
[c] The rough estimation.
[d] Ref. [9].
[e] Refs. [23,24].
[f] Ref. [22].
[g] Ref. [25].
[h] Ref. [26].

The values of $\Gamma_i$, $P_{p1}$, $\varepsilon_{p1}$, $\Gamma_{p1}$, $P_{p2}$, $P_m$ and $\Gamma_m$ in Table 2 were discussed in the previous work [9]. Since the energy of photons from $He_2^*(A^1\Sigma_u^+)$ is considerably larger than that from $He^*$, $\Gamma_{p2}$ is roughly estimated to be 0.1 comparing with the value of 0.01 for $\Gamma_{p1}$. Then, $\varepsilon_{p2}(= R_{p2}/G/P_{p2}/\Gamma_{p2})$ at 4.2 K is calculated to be 0.1. The $\varepsilon_{p2}$ is approximately given by

$$\varepsilon_{p2} = \frac{\lambda_p}{\lambda_p + D_{ot}}, \tag{33}$$

where $\lambda_p$ is the sum of the reaction rates of collisions (2a) and (3a) and $D_{ot}$ is the rate of other competing processes. The value of $\lambda_p$ is about $10^6$ $s^{-1}$ at room temperature, while it is estimated to be $1/(180 \times 10^{-6}) \sim 5.56 \times 10^3$ at 4.2 K because of $T_p = 180$ μs. The parameter $D_{ot}$ at 4.2 K is calculated to be $0.9\ \lambda_p(T = 4.2\text{ K}) \sim 5 \times 10^3$ by using Eq. (31c). If $D_{ot}$ does not depend on the temperature, $\varepsilon_{p2}$ at room temperature is estimated to be 1. Assuming that all of $He^m$ ($2^3S$) are turned to $He_2^m(a^3\Sigma_u^+)$, $\varepsilon_m$ and $\Gamma_m$ at 4.2 K are estimated to be 1 and 0.01, respectively. Similar to $\varepsilon_{p2}, \varepsilon_m$ at room temperature equals to 1. The gas gain $G$ and the $R$ values at room temperature have also been estimated from the results for $P$, $\varepsilon$ and $\Gamma$ values.

As seen from Table 2, $R_i$ and $R_m$ at room temperature are considerably larger than $R_{p1}$ and $R_{p2}$. This indicates that the operation of HFPC at room temperature is mainly harmed by positive ions $He_n^+$ and metastable molecules $He_2^m(a^3\Sigma_u^+)$ rather than photons from $He^*$ and $He_2^*(A^1\Sigma_u^+)$. On the other hand, all $R$ values at 4.2 K are the same order of 0.1–0.5, indicating that all active particles result in the unstable operation of the HFPC at 4.2 K. The parameter $R_i$ is decreased at 4.2 K while $R_{p1}$ is increased. These changes in $R_i$ values come from the suppression of atom–atom or atom–molecular collisional processes at 4.2 K, as discussed in the previous work [9]. The decrease in $R_i$ at 4.2 K results from the decrease in $\Gamma_i$, which is caused by the formation of helium ion clusters [16]. Using Eqs. (9), (10), (14) and (22), the maximum available gas gain at room temperature is calculated to be 5.6, which is considerably smaller

than that at 4.2 K. The favorable increase of the gas gain at 4.2 K mainly comes from the decrease in $\Gamma_i$. The present results in Table 2 clearly show that the unstable operation of the HFPC at 4.2 K is caused by large values of $R_{p2}$ and $R_m$, which result from the creation of a large amount of $He_2^*(A^1\Sigma_u^+)$ and $He_2^m(a^3\Sigma_u^+)$ in electron avalanches, respectively. Note that these excited molecules are produced from metastable atoms, i.e. $He^m(2^1S)$ and $He^m(2^3S)$.

In the simple model for the HFPC operation described in Section 1, all of $He^m$ $(2^3S)$ created in electron avalanches changes to $He_2^m(a^3\Sigma_u^+)$ through collisions with helium gas atoms, i.e. $\varepsilon_m = 1$. The metastable molecules $He_2^m(a^3\Sigma_u^+)$ diffuse to the cathode where they emit electrons with a probability $\Gamma_m(= \sim 0.01)$ at 4.2 K. However, the present simulation of electric discharge in the model does not agree with the experimental data, indicating that triplet metastables $He^m(2^3S)$ and $He_2^m(a^3\Sigma_u^+)$ may have other channels to decay or decompose in the electron avalanches, where the densities of the metastables and electrons are relatively high.

Thus, the triplet metastables $He^m(2^3S)$ and $He_2^m(a^3\Sigma_u^+)$ may create positive ions and electrons or emit photons through the collisions with other metastables or electrons. The higher the anode voltage becomes, the more metastables are created and then their collisional reactions cannot be ignored. Electrons or photons created by the above collisional reactions promote the electric discharge. At the high gas density, the diffusion velocity of $He_2^m(a^3\Sigma_u^+)$ becomes smaller and many of them stay near the anode for a longer time. The rates of collisional reaction described above become higher, and photons and electrons are emitted with higher probabilities in high gas density. Further study for the collisional ionization of $He^m(2^3S)$ and $He_2^m(a^3\Sigma_u^+)$ is apparently necessary to understand the electric discharge.

## 6. Conclusion

A model proposed in our previous work [9] indicated that the operation of HFPC is harmed by four active particles: helium ion clusters $He_n^+$, photons from excited helium atoms $He^*$, photons from excited helium molecules $He_2^*(A^1\Sigma_u^+)$ and metastable helium molecules $He_2^m(a^3\Sigma_u^+)$. As a result of simulating the signal pulses in the present work, it has been proved that the former three particles form the after-pulses, as shown by Figs. 4 and 5. The parameters $R_{p2}$ and $R_m$ were not estimated in the previous works while $R_{p2}$ has been determined from the present simulation. Furthermore, $R_m$ at the maximum available voltage $V_{max}$ has been estimated from Eq. (31b). However, the behavior of the triplet metastables $He^m(2^3S)$ and $He_2^m(a^3\Sigma_u^+)$ in the HFPC operation is still not clear. Taking account of other possible atomic and molecular processes for the metastables, we are now examining the electric discharge with the simulation method.

One of the possible applications for the cryogenic helium-filled proportional counter is a new type of neutron position detector. In the $^3$He-filled counter, which is intensively employed as a neutron counter, a thermal neutron produces a proton, p, and a tritium, $^3$H, through the nuclear reaction. The range of p is much longer than that of $^3$H, which causes a gap between the position of the reaction and that of the center of p and $^3$H. This gap determines the limit of the position resolution. The way to improve the position resolution of the $^3$He-filled proportional counter is to increase the gas density in the counter. It may be possible to obtain the high position resolution of about 1 mm by using the $^3$He-filled proportional counter at 4.2 K with high gas density of 40 atm at room temperature. Since the cross-section of the nuclear reaction is very large, we can use a gas mixture of $^4$He and $^3$He. We are now examining the performance of HFPC at 4.2 K with gas densities corresponding to 20–60 atm at room temperature.

## References

[1] M.J. Tricker, in: J.G. Stevens, G.K. Shenoy (Eds.), Mössbauer Spectroscopy and its Chemical Applications, in: Advances in Chemistry Series no. 194, 1981.
[2] G. Balestrino, in: N.A. Eissa, G. Denardo (Eds.), Proceedings of the School on Applications of Nuclear Gamma Resonance Spectroscopy, World Scientific, Singapore, 1986, p. 159.
[3] G.N. Belozerski, Mössbauer Studies of Surface Layer, Elsevier, Amsterdam, 1993, p. 220.

[4] Y. Isozumi, T. Fujii, Current Topics in Crystal Growth Research, Vol. 1, Research Trends, India, 1994, p. 187.
[5] Y. Isozumi, S. Kishimoto, R. Katano, H. Takekoshi, Rev. Sci. Instr. 58 (1987) 293.
[6] Y. Isozumi, S. Ito, T. Fujii, R. Katano, Rev. Sci. Instr. 60 (1989) 3262.
[7] K. Fukumura, T. Kobayashi, A. Nakanishi, R. Katano, Y. Isozumi, Hyp. Int. 69 (1991) 755.
[8] S. Kishimoto, Y. Isozumi, R. Katano, H. Takekoshi, Nucl. Instr. and Meth. A 262 (1987) 413.
[9] S. Masaoka, R. Katano, S. Kishimoto, Y. Isozumi, Nucl. Instr. and Meth. B 171 (2000) 360.
[10] J.A. Hornbeck, J.P. Molnar, Phys. Rev. 84 (1969) 621.
[11] Y. Isozumi, R. Katano, S. Ito, S. Kishimoto, Nucl. Instr. and Meth. A 355 (1995) 443.
[12] S. Masaoka, R. Katano, Y. Isozumi, Nucl. Instr. and Meth. B 160 (2000) 172.
[13] G.F. Knoll, in: Radiation Detection and Measurement, Wiley, New York, 1989.
[14] A. von Engel, in: Ionized Gas, Clarendon, Oxford, 1965.
[15] E. Kowalski, in: Nuclear Electrons, Springer, Berlin, 1970.
[16] N. Kobayashi, T. Kojima, Kaneko, J. Phys. Soc. Jpn. 57 (1988) 1528.
[17] T. Holstein, Phys. Rev. 72 (1947) 1212.
[18] T. Holstein, Phys. Rev. 83 (1951) 1159.
[19] M.G. Payne, G.S. Hurst, M.H. Nayfeh, J.P. Judish, C.H. Chen, E.B. Wagner, J.P. Young, Phys. Rev. Lett 35 (1975) 1154.
[20] G. Bekefi, Principle of Laser Plasmas, Wiley, New York, p. 212.
[21] G. Myers, A.J. Cunningham, J. Chem. Phys. 67 (1977) 247.
[22] G.D. Alkhazov, A.A. Vorob'ev, Phys. Lett. 29A (1969) 25.
[23] H.D. Hagstrum, Phys. Rev. 89 (1953) 244.
[24] H.D. Hagstrum, Phys. Rev. 96 (1954) 325.
[25] R.F. Stebbings, Proc. R. Soc. A 241 (1957) 270.
[26] A.V. Phelps, Phys. Rev. 99 (1955) 1307.